Processing and Application of Ceramics 17 [4] (2023) 365–373
https://doi.org/10.2298/PAC2304365W

Improving the steel corrosion resistance of calcium hexaaluminate with addition of M_2O_5 (M = Nb, Ta)

Tianpeng Wen[1,2], Zhipeng Wang[1], Yao Jin[1], Jingkun Yu[1], Zhengguo Yan[1], Zhaoyang Liu[1], Lei Yuan[1,2,*]

[1] *School of Metallurgy, Northeastern University, Shenyang, 110819, P.R. China*
[2] *Key Laboratory for Ecological Metallurgy of Multimetallic Mineral (Ministry of Education), Shenyang 110819, Liaoning, PR China*

Received 7 July 2023; Received in revised form 8 November 2023; Accepted 21 November 2023

Abstract

Calcium hexaaluminate (CA_6) materials have garnered attention for their potential use as lining materials in metallurgical furnaces during the steel-making process. The present work explored the effects of M_2O_5 (M = Nb, Ta) on the steel corrosion behaviour of calcium hexaaluminate combined with the evolution of physical properties. The introduction of M_2O_5 (M = Nb, Ta) was proved to be advantageous in mitigating the emulsification of CA_6 material in the molten steel, and the increase in the densification of emulsion layer could prevent CA_6 materials from further steel corrosion and penetration. The improved steel corrosion resistance of CA_6 materials was attributed to the optimization of the physical properties facilitated by the formation of defects and the in situ phase. In addition, the reduction in the wettability between the CA_6 materials and molten steel served to diminish the reactivity of the interface reaction. This work determined the corrosion behaviour and corrosion mechanism of the CA_6 materials in molten steel and provided a new research route for designing CA_6 materials with improved corrosion resistance to molten steel.

Keywords: *calcium hexaaluminate, steel corrosion, physical properties, interface reaction*

I. Introduction

Calcium hexaaluminate ($CaAl_{12}O_{19}$), often referred to as CA_6, has been widely used in metallurgy, petrochemical and various other fields due to its unique physical and chemical properties, including high melting point, excellent high temperature mechanical properties and chemical stability [1–4]. However, CA_6 structure comprises stacked spinel block units and mirror layers in alternating pattern, resulting in a layered structure. This structural arrangement poses challenges in achieving full density for the reaction sintered CA_6 refractories, even at the elevated temperatures [5–11]. Consequently, the CA_6 with porous structure is generally obtained and such structures will allow the steel infiltration into the CA_6 material matrix, which accelerates the degradation of inherent properties. Simultaneously, the corrosion of CA_6 refractories can also adversely affect the iron-making and steelmaking processes.

In the context of refractory applications in iron and steel smelting, it is crucial to predict service performance, stability and reliability. This necessitates a deeper understanding of corrosion behaviours and mechanisms [12–14]. CA_6 plays a vital role in calcium aluminate cements and aluminium magnesium castables for ladle [15–18]. During the initial high temperature use of aluminium magnesium castables, a large amount of CA_6 is generated in the refractory matrix and the development of CA_6 layer structure leads to the increase of porosity of the refractories, resulting in the severe steel penetration phenomenon [16]. Accordingly, the deterioration of the corrosion resistance of refractories will inevitably affect the service performance and service life. In addition, the exfoliation of refractories under the steel erosion leads to an increase in the amount of the external inclusions in the steel, which not only affects the quality of the steel but also results in the submerged nozzle clogging of the molten steel during the continuous casting process [19–21]. Therefore, enhancement of steel resistance is of paramount importance to the

---

[*] Corresponding author: tel: +86 024 83681576,
e-mail: *yuanl@smm.neu.edu.cn*

application of CA_6 materials and other CA_6-containing composite materials. On this basis, exploring the corrosion behaviour and corrosion mechanism of steel towards CA_6 materials will be of great significance for developing new techniques to reduce the steel corrosion.

Different methods were used for preparation of calcium aluminates, and most of them were based on a high-temperature solid-phase method, i.e. solid-state reaction sintering of Al_2O_3 and $CaCO_3$ powder mixtures [22,23]. However, calcium aluminate powders were obtained by wet-chemical synthesis methods too [24–26] and calcium hexaaluminate ceramics were made also from calcium dialuminate (CA_2) and corundum powders [27], CaO, Al_2O_3 and Al powders [3] etc.

Numerous studies have explored the doping with small amount of bivalent, trivalent or tetravalent cations substituting the Ca^{2+} or Al^{3+}, resulting in more V_{Al} defects in the structure of CA_6 and promoting grain development and increasing the density [28–35]. Although many of these studies do not directly address the steel corrosion resistance of CA_6, it is clear that the improvement of CA_6 densification will be beneficial for reducing the steel corrosion. Limited to this, the discussion of corrosion mechanism is insufficient. Moreover, it is foreseeable that dopants with higher-valence state and smaller-size may have potential to generate more V_{Al} than other low valent dopants, thus, the crystal structure of CA_6 and the comprehensive properties can be optimized. Therefore, considering the limited research on the improvement of the properties of the CA_6 materials by doping pentavalent elements, the present work investigates the role of the M_2O_5 (M = Nb, Ta) on the steel corrosion behaviour of CA_6 materials. In order to get the insight into the mechanism of the effects of additives on the CA_6 corrosion resistance to steel, the evolution of physical properties and microstructure of M_2O_5-doped CA_6 materials and the wettability between CA_6 material and steel were explored. This work determines the corrosion behaviour and mechanism of steel influence on CA_6 materials and provides a new research route for the design of CA_6 materials with improved steel corrosion resistance, which will contribute to the better application of CA_6 in metallurgical and petrochemical fields.

II. Experimental

2.1. Sample preparation

The Al_2O_3 (purity ≥99.0%, Sinopharm Chemical Reagent Co. Ltd.) and $CaCO_3$ (purity ≥99.0%, Sinopharm Chemical Reagent Co. Ltd.) powders with the molar ratio of 6:1 were employed as starting materials for the preparation of the CA_6 refractories, whereas Nb_2O_5 (purity ≥99.0%, Sinopharm Chemical Reagent Co. Ltd.) and Ta_2O_5 (purity ≥99.0%, Sinopharm Chemical Reagent Co. Ltd.) were used as the additives. The compositions were ball milled using corundum balls media in ethanol for 4 h and then the ball-milled slurries were dried at 90 °C. The obtained powders were uniaxially pressed into pellets at a pressure of 300 MPa for heat treatment at 1200 °C for 1 h. The obtained samples were crushed and ball milled again for 2 h with Nb_2O_5 and Ta_2O_5 added (1.0 wt.% and 4.0 wt.%), respectively. After drying, specimens of 20 mm in width, 20 mm in height and 100 mm in length were compacted under a pressure of 100 MPa. The specimens were sintered at the peak temperature of 1600 °C for 2 h in air with the heating rate of 5 °C/min. Subsequently, the static crucible test was used to investigate the steel corrosion resistance of the sintered CA_6 specimens. This experiment simulated the actual smelting process and took place under ambient air conditions, where the specimens were heated to the target temperature (1600 °C) at a heating rate of 5 °C/min with the holding time of 2 h. For reference, the CA_6 prepared without an additive was used as the baseline material for comparison with the properties of the prepared specimens. Figure 1 shows schematic presentation of static crucible test, chemical composition of the steel, as well as macro-appearances and compositions of samples with and without additives used in the present study.

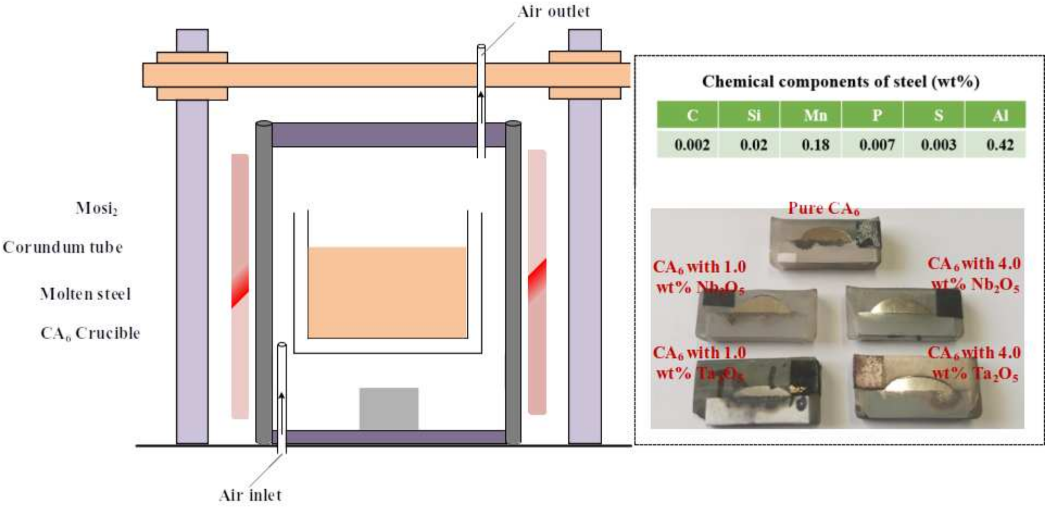

Chemical components of steel (wt%)

C	Si	Mn	P	S	Al
0.002	0.02	0.18	0.007	0.003	0.42

Figure 1. Scheme of static crucible test and the compositions of the steel

2.2. Characterization

The field emission scanning electron microscopy (FE-SEM, Model Ultra Plus, ZEISS, Germany) and the energy dispersive spectroscopy (EDS, Oxford, United Kingdom) were used for analysing the steel corrosion behaviour of prepared CA_6 specimens. The dripping method was adopted to measure the wetting contact angle between the CA_6 specimens and steel.

The phase compositions of the sintered CA_6 specimens were detected using X-ray diffraction (XRD, Model D500, Siemens) using Cu Kα radiation. For the physical properties of the CA_6 samples, the Archimedes principle was adopted to determine the densification parameters in terms of bulk density and apparent porosity based on the water as the medium.

III. Results and discussion

Figure 2 presents the corroded microstructures and EDS mapping analysis of the pure CA_6 (baseline). Observations revealed the presence of three distinct layers: the original steel layer, the corrosion layer, and the original CA_6 layer. Within the corrosion layer, adjacent to the CA_6 substrate, there was a noticeable penetration layer composed of $FeO\text{-}Fe_2O_3\text{-}Al_2O_3$ composite phase and CA_6 phase. The emulsion layer was located between the penetration layer and the original steel layer. It was composed of $FeO\text{-}Fe_2O_3\text{-}Al_2O_3$ composite phase, $CA\text{-}CA_2$ ($CaAl_2O_4\text{-}CaAl_4O_7$) phase, and a low amount of Fe phase. The $FeO\text{-}Fe_2O_3\text{-}Al_2O_3$ composite phase, resulting from the interfacial reaction between molten steel and CA_6, was distributed within the CA_6 material. This distribution of the composite phase effectively delayed further CA_6 corrosion and steel penetration [36–38]. In summary, the thickness of the corrosion layer in the pure CA_6 samples (without additives) was measured to be approximately 1462 µm, comprising of 566 µm for the penetration layer and 896 µm for the emulsion layer.

The SEM images and EDS mapping analysis of the corroded cross-section of the M^{5+}-doped CA_6 (M = Nb, Ta) after corrosion test are displayed in Figs. 3 and 4.

In the case of the Nb^{5+}-doped CA_6, SEM images (Fig. 3) indicate that the thickness of corrosion layer decreased significantly compared to that of pure CA_6, since the thicknesses of corrosion layers were 1061 µm and 439 µm for the CA_6 specimens with 1.0 wt.% and 4.0 wt.% of Nb_2O_5 addition, respectively. The enrichment of molten steel inside the CA_6 materials was significantly reduced, accompanied by a decrease in the thicknesses of the emulsion layer (reducing from 896 µm for pure CA_6 to 386 µm for the doped CA_6 with 4.0 wt.% of Nb_2O_5 addition) and penetration layer (reducing from 566 µm for pure CA_6 to 53.0 µm for the doped CA_6 with 4.0 wt.% of Nb_2O_5 addition). This observation demonstrated that only a slight corrosion of the CA_6 materials was presented and that the steel corrosion resistance of CA_6 materials was greatly improved. The EDS analysis results confirmed that the emulsion layer was composed of $FeO\text{-}Fe_2O_3\text{-}Al_2O_3$ composite phase, $CA\text{-}CA_2$ ($CaAl_2O_4\text{-}CaAl_4O_7$) phase and small amount of penetrated Fe phase. Accordingly, the formed $FeO\text{-}Fe_2O_3\text{-}Al_2O_3$ composite phase distributed in the CA_6 materials further improved the densification of the emulsion layer, resulting in further inhibition of corrosion and infiltration. Because of this, the thickness of the penetration layer sharply decreased compared to that of pure CA_6 materials.

For the Ta^{5+}-doped CA_6, the changes in the emulsion layer and penetration layer exhibited the same trend as the Nb^{5+}-doped CA_6 (Fig. 4), indicating that the steel corrosion resistance of CA_6 materials was also enhanced by introduction of the Ta_2O_5. The thicknesses of corrosion layers (1080 µm and 682 µm for the CA_6 specimen with 1.0 and 4.0 wt.% of Ta_2O_5 addition, respectively) were larger than that of the Nb^{5+}-doped CA_6. The synergetic effect of penetration layer and emulsion

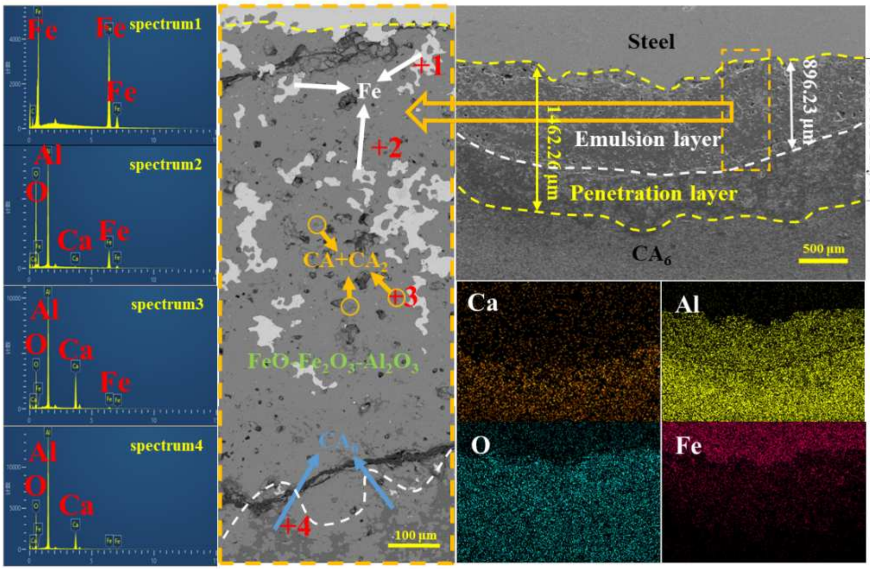

Figure 2. Corroded microstructures and EDS mapping analysis of CA_6 baseline specimen

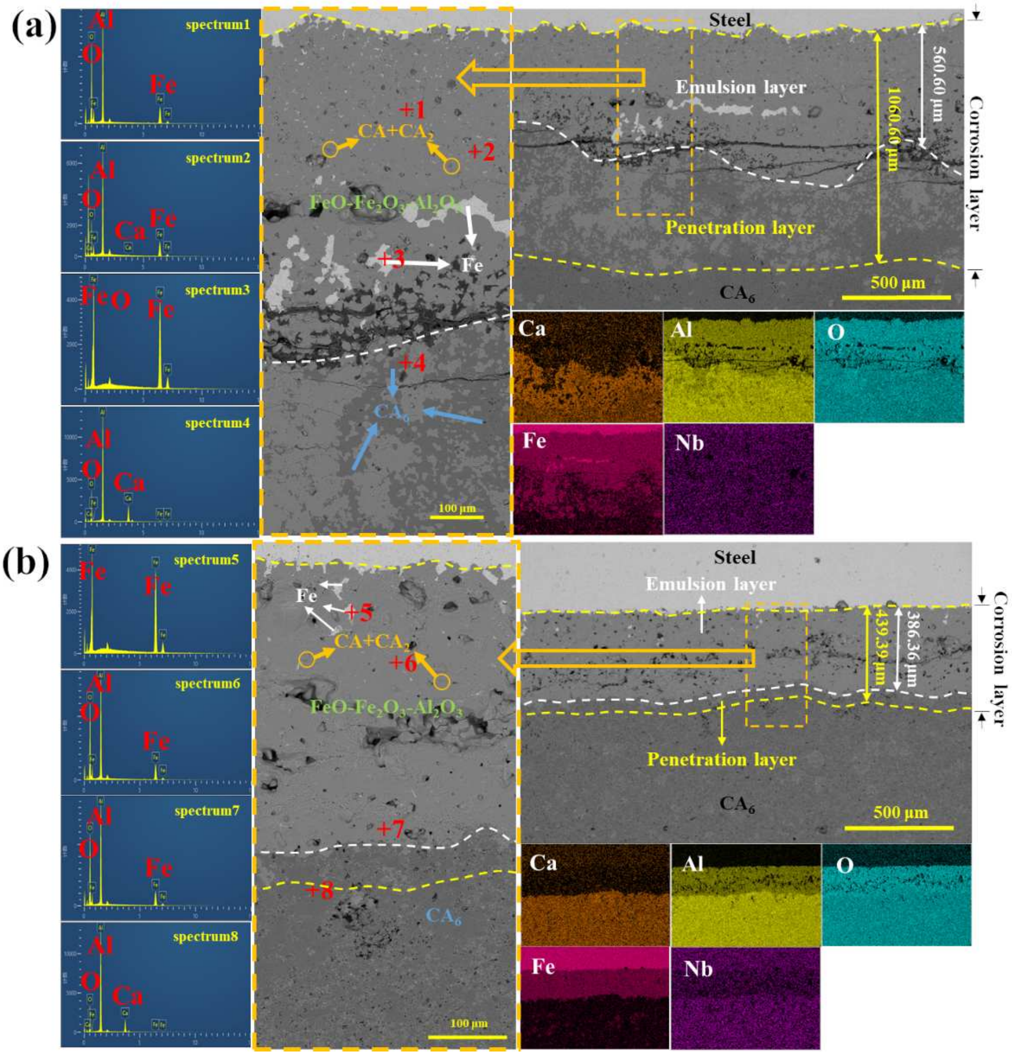

Figure 3. SEM images and EDS mapping analysis after corrosion test of the Nb^{5+}-doped CA_6 with: a) 1.0 wt.% and b) 4.0 wt.% of Nb_2O_5 addition

layer played a crucial role in affecting the steel corrosion resistance of CA_6 materials. For the Nb^{5+}- and Ta^{5+}-doped CA_6, the decrease in the thicknesses of the penetration layer and the emulsion layer significantly contributed to the improvement of the steel corrosion resistance.

Figure 5 summarizes the steel corrosion resistance of the CA_6 materials, which included measurements of the thicknesses of the emulsion layer of CA_6, penetration layer of steel and the total corrosion layer. It is evident that both Nb^{5+}-doped and Ta^{5+}-doped CA_6 samples exhibited a thinner corrosion layers compared to that of the pure CA_6 samples. In summary, it can be affirmed that the steel corrosion resistance of the CA_6 materials was improved after M_2O_5 (M = Nb, Ta) was introduced and the types of the additives had an important effect on the steel corrosion resistance behaviour of CA_6 materials.

In order to clarify the corrosion mechanism of molten steel in the CA_6 materials, Fig. 6 provides the schematic diagram of the reaction between molten steel and CA_6 materials. As depicted in Fig. 6a, the molten steel enters the interior of the CA_6 materials through the pores and cracks on the surface of the materials at the initial stage. Subsequently, the penetrated steel reacts with the CA_6 substrate, forming a liquid interface layer primarily composed of FeO-Fe_2O_3-Al_2O_3 composite phase at high temperatures. The liquid interface layer emulsified with the molten steel under the dynamic conditions, allowing the molten steel to further penetrate into the CA_6 materials accompanied by the reaction and aggregation. The accumulation of the molten steel in the interior of CA_6 materials and the occurred reaction will cause large cracks inside the materials, resulting in the damage at the reaction interface. After the molten steel invades the interior of the material, the new interface of the CA_6 material reacts with the molten steel again, leading to additional damage of the CA_6 material [39].

With the introduction of Nb_2O_5 and Ta_2O_5 into the CA_6 materials, the thickness of the corrosion layer in CA_6 was significantly reduced, as shown in Fig. 6b. In fact, CA_6 lattices serve as an excellent host structures for the formation of solid solutions by substituting Al^{3+}

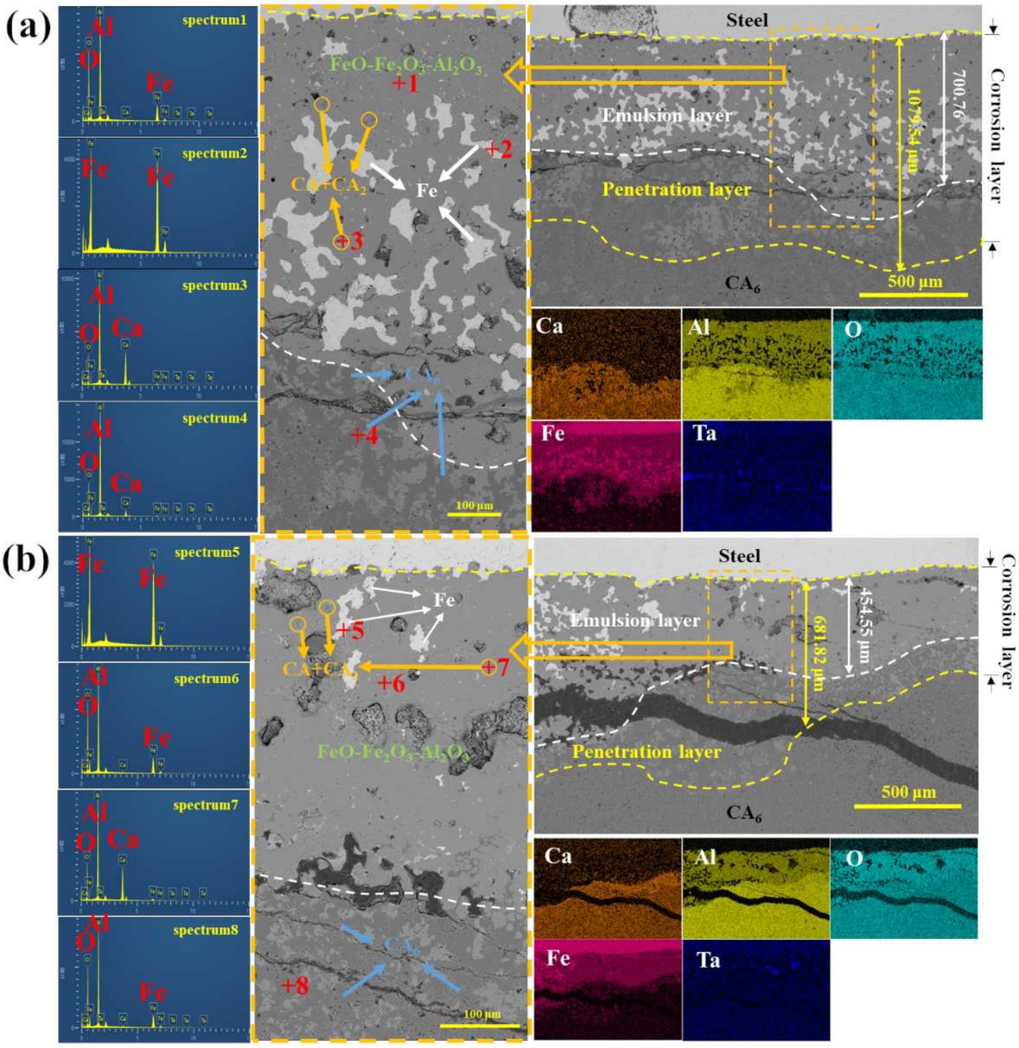

Figure 4. SEM images and EDS mapping analysis after corrosion test of the Ta^{5+}-doped CA_6 with: a) 1.0 wt.% and b) 4.0 wt.% of Ta_2O_5 addition

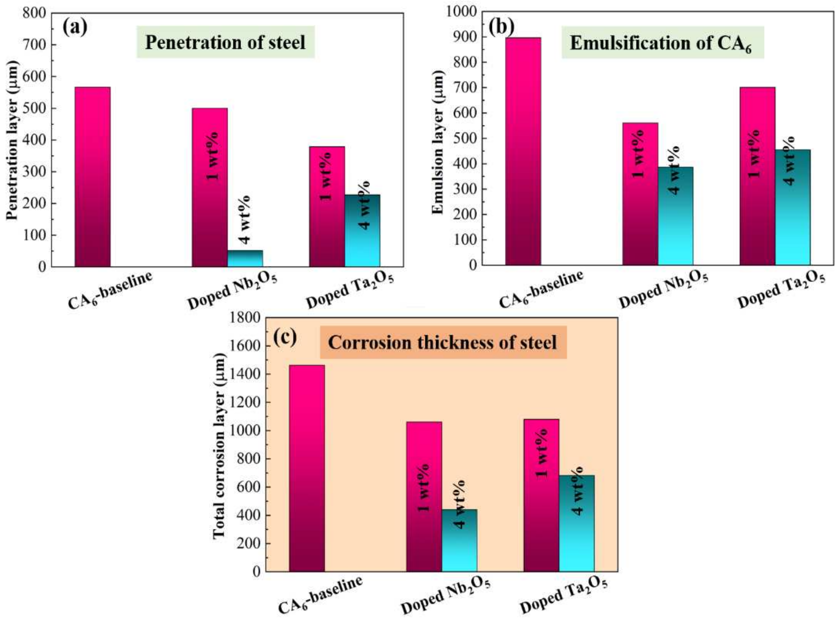

Figure 5. Thickness of the penetration layer of steel, the emulsion layer of CA_6 material and the total corrosion layer

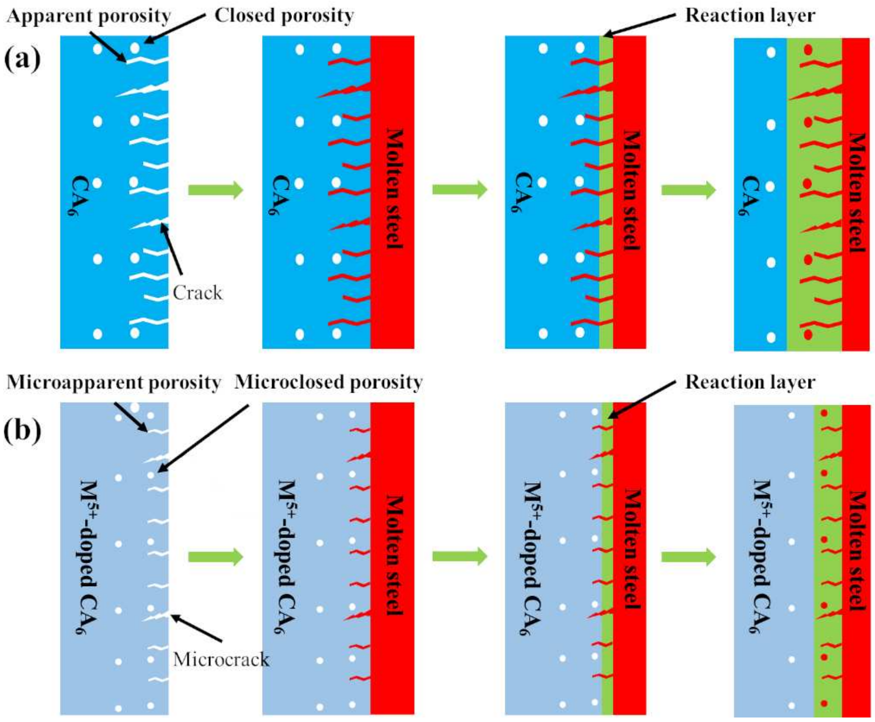

Figure 6. Schematic of the reaction between molten steel and CA_6 materials

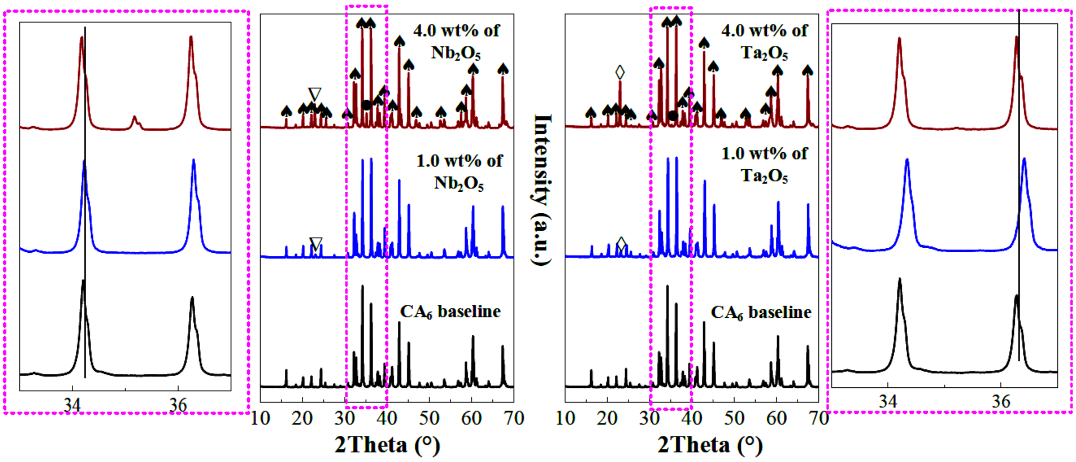

Figure 7. XRD patterns of the sintered CA_6 with various M_2O_5 contents

with metal cations and Ca^{2+} with alkaline-earth or rare-earth cations of similar radii. The XRD patterns of the sintered CA_6 after addition of M_2O_5, shown in Fig. 7, indicated that the introduced M^{5+} substituted Al^{3+} in the CA_6 lattice, caused the formation of V_{Al} defects, according to Pauling's rules, resulting in a reduction in lattice parameters and lattice volume. This substitution of M^{5+} (M = Nb, Ta) for Al^{3+} in CA_6 notably promoted CA_6 grain growth along the direction perpendicular to the basal plane (*c*-axes), resulting in a more equiaxed morphology and a highly dense microstructure [22,40]. Furthermore, formed $Ca(MO_3)_2$ infiltrated the pores within the CA_6 samples and reduced the apparent porosity [22,40]. Based on the above analysis, the introduction of the Nb_2O_5 and Ta_2O_5 significantly improved physical properties of the sintered CA_6 materials, as shown in Fig. 8. The reduction in the apparent porosity diminished the infiltration of molten steel into the interior of the material through surface pores and microcracks. In addition, the additives can play an important role in refining grain size and reducing micro cracks inside the materials, thus the aggregation area of molten steel after infiltration into the interior of the material also decreased. The synergistic effect of two factors alleviated the infiltration and aggregation of molten steel inside the CA_6 materials. Similarly, the formed FeO-Fe_2O_3-Al_2O_3 and CA-CA_2 phases can prevent further penetration of the molten liquid.

It is worth noting that the wettability between molten steel and CA_6 materials was also a significant factor that affected the steel corrosion resistance of CA_6 materials. Figure 9 illustrates the wetting behaviour of molten steel

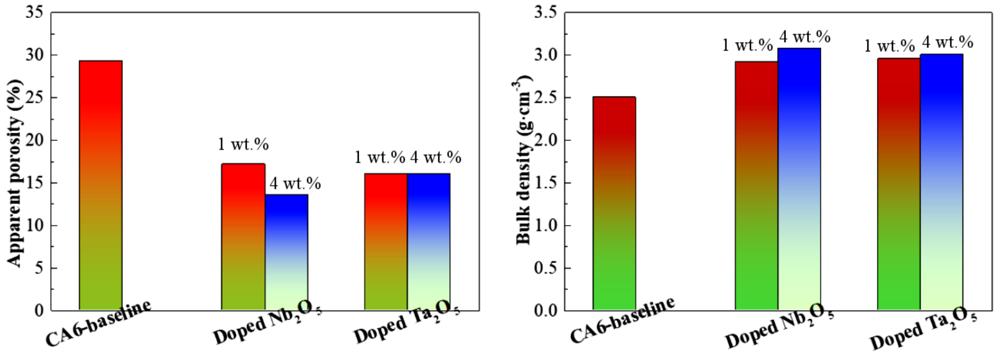

Figure 8. Physical properties of the sintered CA_6 materials

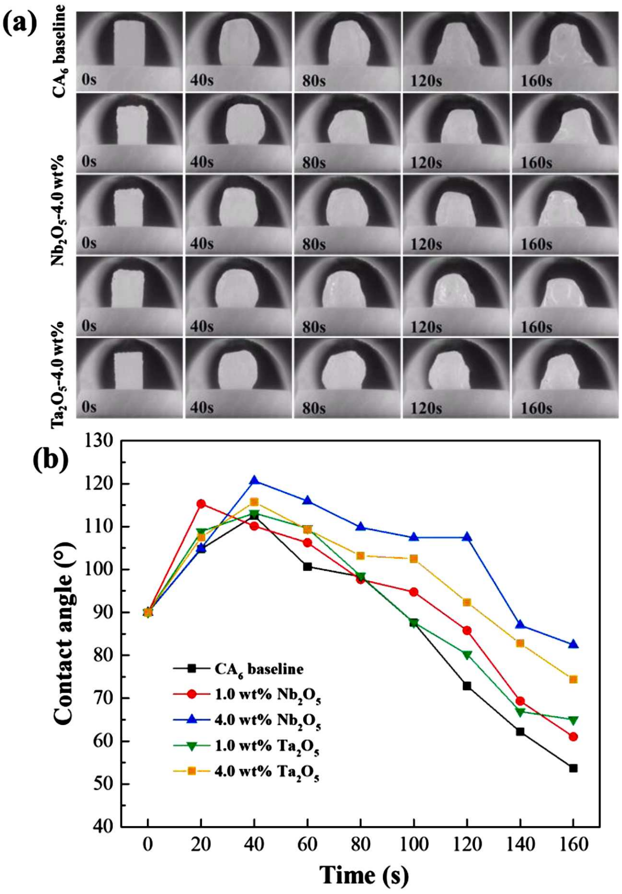

Figure 9. Wetting processes of molten steel on specimens surface (a) and contact angle between CA_6 specimens and molten steel (b)

on the surface of CA_6 with different additives. The high-temperature wetting angle was determined from the moment when the molten steel began to melt, capturing image of the steel every 40 s as shown in Fig. 9a. It is evident that the wetting angle between the pure CA_6 specimen and the molten steel was significantly smaller than that of the specimens with the additives (Nb_2O_5, Ta_2O_5) added. Figure 9b shows the changes in wetting angle between the molten steel and the CA_6 specimens. Considering the accuracy of the experiment, the wetting angle was measured at a node of 20 s. The wetting angle between the pure CA_6 specimen and the molten steel reached maximum within 40 s, reaching 112.5°. After 120 s, the wetting angle decreased to 53.7° (a reduction of about 52.3%). After adding 1.0 wt.% and 4.0 wt.% Nb_2O_5, the wetting angles between the CA_6 specimen and the molten steel reached a maximum of 115.3° and 120.65° within 40 s, respectively. After 120 s, the wetting angles decreased to 61° and 82.45° (a reduction of about 47.1% and 31.6%, respectively). Similarly, the wetting angles between the sample and the molten steel reached a maximum of 113.15° and 115.75° within 40 s when 1.0 wt.% and 4.0 wt.% Ta_2O_5 were added to the CA_6 specimen, respectively. After 120 s, the wetting angles decreased to 65° and 74.35° (a reduction of about 42.6% and 35.7%, respectively). The above analysis indicates that the presence of additives reduced the wettability between molten steel and CA_6 materials. This decreases the reactivity between the molten steel and the materials, thereby reducing the corrosion of the molten steel in the CA_6 material.

In summary, the key factors contributing to the reduction in CA_6 corrosion by molten steel included low porosity, decreased wettability and the formation of the secondary phases. The introduction of Nb_2O_5 and Ta_2O_5 into the CA_6 enhanced the material's physical properties by promoting defect formation and *in situ* phase formation. This improvement was beneficial for reducing emulsification and penetration of molten steel into CA_6 samples. In addition, the formation of dense FeO-Fe_2O_3-Al_2O_3 and CA-CA_2 phases effectively inhibited further corrosion by the molten steel.

IV. Conclusions

The present work looked at the role of the M_2O_5 (M = Nb, Ta) on the steel corrosion behaviour of CA_6 materials. The evolution of physical properties and microstructure of M^{5+}-doped CA_6 materials and the wettability between CA_6 materials and steel were combined in order to explore the effects of the additives on the steel corrosion resistance of CA_6 materials. It was found that the introduction of Nb_2O_5 and Ta_2O_5 was beneficial for reducing the emulsification of CA_6 material in the molten steel, whereas the increase in the densification of emulsion layer could prevent CA_6 materials from further steel corrosion and penetration. The improvement in the steel corrosion resistance of the Nb^{5+}- and Ta^{5+}-

doped CA_6 materials were attributed to the optimization of physical properties caused by the point defects and the *in situ* phase formations. In addition, the reduction in the wettability between the CA_6 materials and molten steel decreased the reactivity at the CA_6-steel interface. Among the tested compositions, the Nb^{5+}-doped CA_6 exhibited the best physical properties and thereby possessed the satisfactory steel corrosion resistance. This work determined the behaviour and mechanism of steel corrosion on CA_6 materials and provided a new research route for the design of CA_6 materials with improved steel corrosion resistance. These findings have the potential to enhance the efficacy of CA_6 in metallurgical furnaces, thereby improving their overall performance.

Acknowledgements: This work was financially supported by the National Natural Science Foundation of China ((No. 52204337 and No. 52074070), the National Key Research and Development Program of China (2021YFB3701404), China Postdoctoral Science Foundation (No. 2021M700731) and the Fundamental Research Funds for the Central Universities (No. N2225035).

References

1. A. Altay, C.B. Carter, P. Rulis, W.-Y. Ching, I. Arslan, M.A. Gülgün, "Characterizing CA_2 and CA6 using ELNES", *J. Solid State Chem.*, **183** [8] (2010) 1776–1784.
2. V.K. Singh, K.K. Sharma, "Low-temperature synthesis of calcium hexa-aluminate", *J. Am. Ceram. Soc.*, **85** [4] (2002) 769–772.
3. L.C. Xu, E.H. Wang, X.M. Hou, J.H. Chen, Z.J. He, T.X. Liang, "Effect of incorporation of nitrogen on calcium hexaaluminate", *J. Eur. Ceram. Soc.*, **40** [15] (2020) 6155–6161.
4. C. Dominguez, J. Chevalier, R. Torrecillas, L. Gremillard, G. Fantozzi, "Thermomechanical properties and fracture mechanisms of calcium hexaluminate", *J. Eur. Ceram. Soc.*, **21** (2001) 907–917.
5. N. Iyi, S. Takekawa, S. Kimura, "Crystal chemistry of hexaaluminates: β-alumina and magnetoplumbite structures", *J. Solid State Chem.*, **83** (1989) 8–19.
6. D. Holtstam, "Iron in hibonite: a spectroscopic study", *Phys. Chem. Miner.*, **23** (1996) 452–460.
7. R. Salomãoa, V.L. Ferreira, L.M.M. Costa, I.R.D. Oliveira, "Effects of the initial CaO-Al_2O_3 ratio on the microstructure development and mechanical properties of porous calcium hexaluminate", *Ceram. Int.*, **44** (2018) 2626–2631.
8. L.M.M. Costa, J. Sakihama, R. Salomão, "Characterization of porous calcium hexaluminate ceramics produced from calcined alumina and microspheres of Vaterite (μ-$CaCO_3$)", *J. Eur. Ceram. Soc.*, **38** (2018) 5208–5218.
9. T. Nagaoka, T. Tsugoshi, Y. Hotta, M. Yasuoka, K. Watari, "Forming and sintering of porous calcium-hexaaluminate ceramics with hydraulic alumina", *J. Mater. Sci.*, **41** (2006) 7401–7405.
10. F. Zhao, T.Z. Ge, L.X. Zhang, E.X. Xu, J.X. Gao, X.H. Liu, "A novel method for the fabrication of porous calcium hexaluminate (CA_6) ceramics using pre-fired CaO/Al_2O_3 pellets as calcia source", *Ceram. Int.*, **46** (2020) 4762–4770.
11. B. Hallstedl, "Assessment of the CaO-Al_2O_3 system", *J. Am. Ceram. Soc.*, **73** (1990) 15–23.
12. E.D. Bilbao, M. Dombrowski, H. Pillière, J. Poirier, "Time-resolved high-temperature X-ray diffraction for studying the kinetics of corrosion of high-alumina refractory by molten oxides", *Corros. Sci.*, **139** (2018) 346–354.
13. R. Sauerbrey, G. Mori, C. Majcenovic, H. Harmuth, "Corrosion protection of MgO electrodes at 1400 °C", *Corros. Sci.*, **51** (2009) 1–5.
14. J.F. Chen, L.G. Chen, Y.W. Wei, N. Li, S.W. Zhang, "Corrosion and penetration behaviors of slag/steel on the corroded interfaces of Al_2O_3-C refractories: role of Ti_3AlC_2", *Corros. Sci.*, **143** (2018) 166–176.
15. M.W. Vance, G.W. Kriechbaum, R.A. Henrichsen, G. Maczura, K. Moody, S. Munding, "Influence of spinel additives on high-alumina/spinel castables", *Am. Ceram. Soc. Bull.*, **73** [11] (1994) 70–74.
16. J.M. Auvray, C. Gault, M. Huger, "Evolution of elastic properties and microstructural changes versus temperature in bonding phases of alumina and alumina-magnesia refractory castables", *J. Eur. Ceram. Soc.*, **27** (2007) 3489–3496.
17. B.A. Vázquez, P. Pena, A.H. de Aza, M.A. Sainz, A. Caballero, "Corrosion mechanism of polycrystalline corundum and calcium hexaluminate by calcium silicate slags", *J. Eur. Ceram. Soc.*, **29** [8] (2009) 1347–1360.
18. L. Xu, M. Chen, L.Y. Jin, X.L. Yin, N. Wang, L. Liu, "Effect of ZrO_2 addition on densification and mechanical properties of $MgAl_2O_4$-$CaAl_4O_7$-$CaAl_{12}O_{19}$ composite", *J. Am. Ceram. Soc.*, **98** (2015) 4117–4223.
19. E. Roos, A. Karasev, P.G. Jönsson, "Effect of Si and Ce contents on the nozzle clogging in a REM alloyed stainless steel", *Steel Res. Int.*, **86** (2015) 1279–1288.
20. C. Tian, L. Yuan, Y. Li, H.B. Li, T.P. Wen, G.Q. Liu, J.K. Yu, H.X. Li, "Interface reaction between alloys and submerged entry nozzle controlled by an electric current pulse", *Ceram. Int.*, **47** [20] (2021) 28226–28236.
21. C. Tian, L. Yuan, Y. Li, D.B. Jia, T.P. Wen, G.Q. Liu, J.K. Yu, H.X. Li, "Applied electric field on the reaction between submerged entry nozzle and alloy in the steel", *Ceram. Int.*, **47** [16] (2021) 22646–22653.
22. T. Wen, Y. Jin, Z. Yan, Z. Liu, J. Yu, L. Yuan, G. Yuan, "Optimization design of Ta_2O_5-doped calcium hexaaluminate with improved sintering densification and properties for metallurgical application", *J. Alloys Compd.*, **945** (2023) 169297.
23. S. Cui, Q.Wang, Y. Zhou, D. Mao, J. Bao, X. Song, "Effect of nickel oxide and titanium oxide on the microstructural, optical, and mechanical properties of calcium hexaaluminate ceramics", *Ceram. Int.*, **47** (2021) 35302.
24. A.A. Amer, H. El-Didamony, T.M. El-Sokkary, M.I. Wahdan, "Synthesis and characterization of some calcium aluminate phases from nano-size starting materials", *Bol. Soc. Esp. Ceram. Vidrio*, *61* (2022) 98.
25. T. Wen, Y. Jin, C. Tian, L. Yuan, J. Yu, "Synthesis of calcium aluminate powders by ethanol thermal decomposition method", *Process. Appl. Ceram.*, **15** (2021) 403–409.
26. E.V. Ilyina, Y.Y. Gerus, S.V. Cherepanova, A.F. Bedilo, "Synthesis of C12A7 calcium aluminate aerogels", *Mater. Lett.*, **293** (2021) 129699.
27. A. Pięta, M.M. Bućko, M, Januś, J. Lis, S. Jonas, "Calcium hexaaluminate synthesis and its influence on the properties of CA_2-Al_2O_3-based refractories", *J. Eur. Ceram. Soc.*, **35** (2015) 4567.

28. J.H. Chen, H.Y. Chen, W.J. Mi, Z. Cao, B. Li, C.J. Liang, "Substitution of Ba for ca in the structure of $CaAl_{12}O_{19}$", *J. Am. Ceram. Soc.*, **100** [1] (2017) 413–418.
29. Z. Cormack, "Defects in $BaMgAl_{10}O_{17}:Eu^{2+}$ blue phosphor", *J. Electroceram.*, **10** [3] (2003) 179–191.
30. P.M. Doyle, P.F. Schofield, A.J. Berry, A.M. Walker, K.S. Knight, "Substitution of Ti^{3+} and Ti^{4+} in hibonite ($CaAl_{12}O_{19}$)", *Am. Mineral.*, **99** [7] (2014) 1369–1382.
31. L. Liu, T. Onda, Z. Chen, "Microstructural evolution of Ti^{4+}-doped calcium hexaaluminate ceramics", *Ceram. Int.*, **46** (2020) 12897–12901.
32. J. Lu, Y.X. Pan, J.G. Wang, X.A. Chen, S.M. Huang, G.K. Liu, "Reduction of Mn^{4+} to Mn^{2+} in $CaAl_{12}O_{19}$ by co-doping charge compensators to obtain tunable photoluminescence", *RSC Adv.*, **3** [14] (2013) 4510–4513.
33. X.D. Luo, D.L. Qu, Z.P. Xie, X.S. Wang, L.L. Zhang, "Effect of CeO_2 on properties of calcium-hexaluminate material", *J. Mater. Heat Treat.*, **34** [12] (2013) 24–29.
34. T.P. Wen, L. Yuan, E.D. Jin, T. Liu, C. Tian, J.K. Yu, "Effect of CeO_2 addition on the sintering behavior of the alumina-rich calcium aluminate ceramics", *Int. J. Appl. Ceram. Technol.*, **17** (2020) 1761–1768.
35. C.Y. Guo, E.H. Wang, X.M. Hou, J.Y. Kang, T. Yang, T.X. Liang, G.P. Bei, "Preparation of Zr^{4+} doped calcium hexaaluminate with improved slag penetration resistance", *J. Am. Ceram. Soc.*, **104** [9] (2021) 4854-4866.
36. L.P. Fu, Y.S. Zou, A. Huang, H.Z. Gu, H.W. Ni, "Corrosion mechanism of lightweight microporous alumina-based refractory by molten steel", *J. Am. Ceram. Soc.*, **102** (2019) 3705–3714.
37. L. Zhang, "Nucleation, growth, transport, and entrapment of inclusions during steel casting", *JOM*, **65** [9] (2013) 1138–1144.
38. J.K. Yu, A. Yamaguchi, "Mechanism of metal precipitating in alumina grain in sintered Al_2O_3-C", *J. Ceram. Soc. Jpn.*, **103** (1995) 370–373.
39. A. Huang, Y.J. Wang, Y.S. Zou, H.Z. Gu, L.P. Fu, "Dynamic interaction of refractory and molten steel: Corrosion mechanism of alumina-magnesia castables", *Ceram. Int.*, **44** [12] (2018) 14617–14624.
40. T.P. Wen, Y. Jin, J.K. Yu, Z.G. Yan, Z.Y. Liu, L. Yuan, "Effect of Nb_2O_5 additive on the sintering behavior and properties of calcium hexaluminate", *Constr. Build. Mater.*, **385** (2023) 131534.